Design and Analysis of a Redundantly Actuated Parallel Mechanism for Rapid Machining

Jongwon Kim, Frank Chongwoo Park, Sun Joong Ryu, Jinwook Kim, Jae Chul Hwang, Changbeom Park, and Cornel C. Iurascu

***Abstract*—This paper describes the design, construction, and performance analysis of the Eclipse, a redundantly actuated six-degree-of-freedom parallel mechanism intended for rapid machining. The Eclipse is a compact mechanism capable of performing five-face machining in a single setup while retaining the advantages of high stiffness and high accuracy characteristic of parallel mechanisms. We compare numerical and algebraic algorithms for the forward and inverse kinematics of a class of the Eclipse and formalize the notion of machine tool workspace. We also develop a simple method for the first-order elasto-kinematic analysis of parallel mechanisms that is amenable to design iterations. A complete characterization of the singularities of the Eclipse is given, and redundant actuation is proposed as a solution. The Eclipse case study demonstrates how diverse analytical tools originally developed in a robotics context can be synthesized into a practical design methodology for parallel mechanisms.**

***Index Terms*—Overactuation, parallel mechanism, rapid machining, singularity.**

I. Introduction

PARALLEL mechanisms such as the Stewart–Gough platform are receiving widespread attention within the robotics community (see, e.g., [1] for a recent survey and list of references), in applications ranging from high-speed manipulation (e.g., [2]) to force-torque sensing [3]. Because the moving platform is actuated in parallel by several "simple" serial mechanisms, parallel mechanisms are in general capable of very fast and accurate motions, possess higher average stiffness characteristics throughout their workspace, and can carry heavier payloads than their serial counterparts. Their modular structure also makes them quite economical to manufacture. Driven by these potential cost and performance advantages, parallel mechanisms have been receiving increasing attention within the manufacturing community, primarily as platforms for CNC machining; recently, several machine tool manufacturers have developed commercial machining centers based on the Stewart–Gough platform architecture (see, e.g., Valenti [4], Kim *et al.* [5] and the references cited).

Manuscript received January 10, 2000; revised March 5, 2001. This paper was recommended for publication by Associate Editor A. Maciejewski and Editor S. Salcudean upon evaluation of the reviewer's comments. This work was supported in part by the Center for Order-Adaptive Rapid Product Development (OARPD), the BK21 program in Mechanical Engineering at Seoul National University, and the SNU Institute for Advanced Mechinery and Design, by the Engineering Research Center for Advanced Control and Instrumentation at Seoul National University.

The authors are with the School of Mechanical and Aerospace Engineering, Seoul National University, Seoul 151-742, Korea.

Publisher Item Identifier S 1042-296X(01)08892-9.

A closer examination of the machining process reveals that a major bottleneck in reducing machining lead-time is the lengthy workpiece setup time. Since the spindle axis direction is fixed either vertically or horizontally in conventional CNC machines, machining all five faces of a cubic workpiece, for example, usually requires that the workpiece be set up several times. Existing five-face machining centers, consisting of a serial structure together with a rotating worktable, although deceptively simple in appearance, in fact possess a very complicated internal structure—a large amount of experience is embodied in the design and manufacture of the spindle housing unit, which consists of numerous gearing and transmission mechanisms arranged to meet the stringent stiffness and accuracy requirements of machining. The high cost of these machines can be traced in large part to their high mechanical complexity and lack of modularity.

Existing parallel mechanisms, on the other hand, while mechanically simple and modular in structure, are ineffective for five-face machining because of their restricted workspace—as a result of joint range limits and link interference, the moving platforms of these mechanisms can rarely tilt beyond 40 degrees from the horizontal home position. To address the limitations of current parallel mechanisms, we propose in this paper a redundantly actuated, six-degree-of-freedom parallel mechanism, referred to as the Eclipse, that is designed expressly for five-face machining. The unique feature of this mechanism is that the spindle axis can tilt continuously from the horizontal to the vertical and can also continuously sweep 360 degrees over the lateral surfaces of the workpiece. With such a machine, one can now perform not only milling, but also turning, grinding, and other machining processes in a single setup (see Fig. 1)—in effect, a complete machining-based prototyping system can be realized.

Not surprisingly, the design of a machining system involves many of the same issues one confronts when designing robot systems. There exist a large array of analytical tools developed for the performance analysis and design of robot systems, e.g., the notions of manipulability and stiffness ellipsoids, methods for workspace analysis, and algorithms for finding and classifying kinematic singularities. Although the performance requirements for machine tools are inherently different from those for robots, we show that these same analytical tools, when properly modified to reflect the needs of machining, can be used effectively in the design and performance enhancement of parallel mechanism machine tools like the Eclipse. Some care is required, however, because there are numerous subtleties associated with the design of parallel mechanisms, e.g., the existence of different types of kinematic singularities, presence of passive

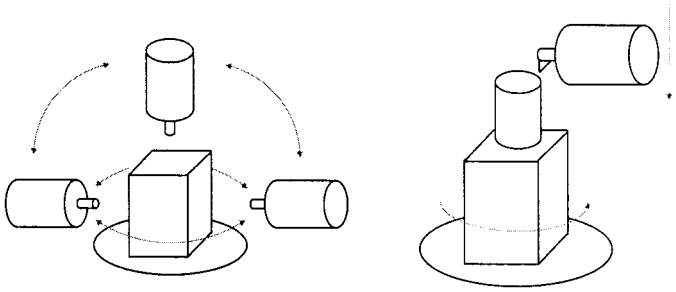

Fig. 1. Prerequisites for a rapid machining center.

joints, different levels of stiffness characterization, link interference, the nature of joint limits, etc.

With these objectives in mind, the main contributions of this paper can be summarized as follows.

- **Efficient algorithms for the forward and inverse kinematic analysis of the Eclipse:** We present both a numerical approach based on Newton–Raphson and an algebraic approach based on dialytic elimination, for solving the forward kinematics of the Eclipse. The performance of the two approaches is also compared.
- **Formulation of the concept of machine tool workspace:** Traditional robotic notions of workspace are not well-suited to machine tools, since one is interested primarily in the direction of the spindle axis—the spindle need not be able to assume general orientations at arbitrary points of the workspace. In this paper, we make precise the notion of a mechanism's *positioning workspace* for a given spindle tilting angle that is designed to take into account the special features of machining tasks. The workspace of the Eclipse is also analyzed using this concept.
- **A methodology for the elasto-kinematic analysis of parallel mechanisms:** The structural stiffness of a mechanism is affected both by joint and link deflections. Although in principle a finite-element analysis will reveal more or less complete information about the mechanism's elastic properties, such an analysis is not only computationally expensive and time-consuming, but also not amenable to design iteration or optimization of a parallel mechanism over the entire range of its workspace. Adopting the Eclipse as a case study, we present a methodology for the first-order stiffness analysis of parallel mechanisms and other closed chain systems that exploits the uniformity and structure extant in parallel mechanisms and is simple enough to be amenable to design iteration. By way of our analysis, we also formalize the notion of a mechanism's structural compliance matrix. Our approach can be viewed as one in which elastic and kinematic effects are addressed on an even footing.
- **A complete characterization of kinematic singularities for parallel mechanisms, and redundant actuation as a general solution:** Parallel mechanisms that possess the complete range of singularities are rare, because joint limits and link interference usually prevent the workspace from being large enough to include the complete variety of possible singularities. The Eclipse is a unique exception. Adopting the singularity classification framework of [6], we identify both actuator and end-effector singularities for the Eclipse; the latter class of singularities has for the most part been overlooked in the literature. The Eclipse possesses an unavoidable actuator singularity within the 0°–90° tilting range; we show how adding an extra actuator can eliminate this and other actuator singularities.[1]
- **An in-depth case study on the design and development of a novel parallel mechanism:** Above all, the Eclipse represents a new—and, to our knowledge, the first—realization of a five-face machining system based on the parallel mechanism concept. The architecture retains most of the intrinsic advantages associated with parallel mechanisms and is designed to fill the niche between conventional machining technology and nonmachining-based rapid prototyping systems. Our case study demonstrates how diverse analytical tools originally developed in a robotics context can be synthesized into a practical design methodology for parallel mechanisms. The case study also underscores the gap between purely theoretical studies and the real-life issues and subtleties one encounters when designing practical parallel mechanisms, e.g., kinematic singularities, factors determining machine stiffness, the effect of joint limits and other hardware considerations. Several new and open research issues are also raised.

The paper is organized as follows. In Section II, we describe the design evolution of the Eclipse and algebraic and numerical solutions to its forward and inverse kinematics. Section III presents a singularity analysis of the Eclipse, including redundant actuation as a means of eliminating singularities, while Section IV presents a workspace analysis from a machining perspective. Section V presents a methodology for the elasto-kinematic analysis of parallel mechanisms. Section VI discusses the development of and experiments with a hardware prototype version of the Eclipse. We conclude in Section VII with a summary and a list of what we feel to be fruitful topics for future research in parallel mechanisms.

II. Kinematic Analysis

This section describes the topological kinematic design of the Eclipse, followed by a procedure for obtaining the closed-form solution of the inverse kinematics, and an algebraic method of the forward kinematics based on dialytic elimination.

A. Conceptual Design

Fig. 2 outlines the conceptual design evolution of the Eclipse. The four designs all share the common topological characteristic of having the moving platform connected to the stationary base by three serial kinematic chains, with two joints of each chain actuated. Intuitively, reducing the number of serial kinematic chains from the typical six to three has the effect of enlarging the workspace and reduces the possibility of link interference, although at a price in reduced machine stiffness. The top two mechanisms are unable to tilt due to limits on the spherical joints. The lower right mechanism, while capable of five-face machining, presents difficulties with respect to manufacturing due to its spherical structure.

[1]Recently, the authors of [7] have also independently investigated the use of additional actuators as a means of eliminating kinematic singularities.

Fig. 2. Conceptual design evolution of the Eclipse.

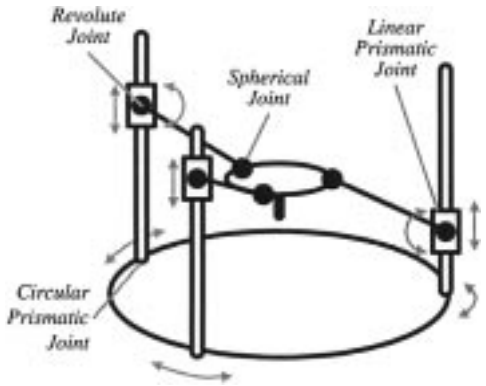

Fig. 3. Final design of the Eclipse.

As shown in Fig. 3, the final Eclipse design consists of three PPRS serial subchains (P, R, and S here denote prismatic, revolute, and spherical joints), with the first P joint denoting sliding motion along the circular guideway. The mechanism has six kinematic degrees of freedom, with the principal actuated joints indicated by arrows. Observe that one of the vertical columns is assembled such that it lies under the circular guideway; this ensures that the links will not interfere with the spindle motor, which protrudes from the upper surface of the moving plate.

B. Inverse Kinematic Analysis

The inverse kinematics problem is to determine the values of the actuated joints from the position and orientation of the tool frame attached to the moving plate. For the Eclipse, its inverse kinematics can be solved by successively solving the inverse kinematics of each subchain. The algorithm for solving the inverse kinematics is as follows.

1) Given the position and orientation of the tool frame, find the Cartesian position of the three spherical joints:

$$P^i = \mathbf{R}\,\overline{P}^{\,i} + P^c$$
$$\overline{P}^{\,i} = \begin{bmatrix} R_w \cos\left(\frac{2}{3}(i-1)\pi\right) & R_w \sin\left(\frac{2}{3}(i-1)\pi\right) & 0 \end{bmatrix}^T$$

where

R_w	radius of the moving platform;
$\overline{P}^{\,i}$	position of the ith spherical joint in tool frame coordinates;
$\mathbf{R}$, P^c	orientation and position of the tool frame in fixed frame coordinates, respectively.

2) From P^i, calculate all relevant joint values as follows:

$$\theta_i = a\tan 2(P_y^i, P_x^i)$$
$$\theta_{i+6} = \cos^{-1}\left(\frac{R_b - \sqrt{P_x^{i2} + P_y^{i2}}}{L}\right) \quad (1)$$
$$\theta_{i+3} = P_z^i - L\sin(\theta_{i+6}) \quad (2)$$

where

$(\theta_1, \theta_2, \theta_3)$	circular prismatic joint values;
$(\theta_4, \theta_5, \theta_6)$	linear prismatic joint values attached to the vertical columns;
$(\theta_7, \theta_8, \theta_9)$	revolute joints attached to the vertical columns [joints $(\theta_1, \theta_4, \theta_7)$ and $(\theta_2, \theta_5, \theta_8)$ correspond to the two serial structures assembled above the circular guide—see Fig. 3];
(P_x^i, P_y^i, P_z^i)	coordinate values of P^i;
R_b, L	radius of the fixed circular guide and the length of the link connecting the moving platform with each vertical column, respectively.

The negative of the value obtained in (2) is also an admissible solution with the following physical interpretation: for positive values, the link is aligned upward (i.e., above the moving platform), while for negative values the link is aligned downward. The sign of the solution obtained in (2) should be inverted for the third vertical column lying under. Also, in (1), another possible solution is given by the given solution plus π. However, here too link interference eliminates the possibility of this particular solution. Existence of the inverse kinematics solution can be established in a trivial way from (2).

C. Forward Kinematic Analysis

The forward kinematics problem is to determine the position and orientation of the tool frame given the values for the actuated joints. As is typical of most parallel mechanisms, in general the forward kinematics solution is not unique, and it is quite difficult to solve the forward kinematics analytically. This section describes both numerical and algebraic approaches for the Eclipse forward kinematics, and a comparison of the performance of the two approaches.

Numerical Approach: In the numerical approach, we employ conventional numerical techniques like the Newton–Raphson method to solve the kinematic constraint equations for the active joint values. The position and orientation of the tool frame can then be easily found from the active and passive joint values.

1) From the requirement that the distances between the spherical joints of the moving platform are fixed, define

TABLE I
COMPARISON OF THE COMPUTATIONAL COST OF THE TWO APPROACHES

approach	computation time	perturbed value	convergence rate	average iteration count
numerical	0.064 msec	rand(0.1π)	99.29 %	7.33
	0.117 msec	rand(π)	97.04%	10.96

approach	computation time	process	CPU time share
algebraic	1.623 msec	finding coefficients of resultant	18.47%
		finding roots of resultant	71.29%
		eliminating imaginary solution	10.24%

the kinematic constraint equations g: $\mathbb{R}^9 \rightarrow \mathbb{R}^3$ as follows:

$$g(\theta_a, \theta_p) = \frac{1}{2}\begin{bmatrix} \|P^1 - P^2\|^2 - D^2 \\ \|P^2 - P^3\|^2 - D^2 \\ \|P^3 - P^1\|^2 - D^2 \end{bmatrix} = \begin{bmatrix} 0 \\ 0 \\ 0 \end{bmatrix}$$

$$P^i = \begin{bmatrix} \cos(\theta_i)(R_b - L\cos(\theta_{i+6})) \\ \sin(\theta_i)(R_b - L\cos(\theta_{i+6})) \\ \theta_{i+3} + L\sin(\theta_{i+6}) \end{bmatrix} \quad (3)$$

where $D = \sqrt{3}R_w$, $\theta_a = [\theta_1, \theta_2, \theta_3, \theta_4, \theta_5, \theta_6]$ (the active joints), and $\theta_p = [\theta_7, \theta_8, \theta_9]$ (the passive joints).

2) Given θ_a, find the passive joint value θ_p that satisfies the above constraint equations. Analytic differentiation of (3) is straightforward, and numerical techniques like the Newton–Raphson method can readily be employed.
3) From the obtained values of the active and passive joints, find the vector P^c and rotation matrix $\mathbf{R}$ representing the position and orientation of the tool frame as follows:

$$P^c = \frac{1}{3}(P^1 + P^2 + P^3)$$
$$\mathbf{R} = [\mathbf{R_x} \quad \mathbf{R_y} \quad \mathbf{R_z}]$$
$$\mathbf{R_x} = \frac{1}{R_w}(P^1 - P^c)$$
$$\mathbf{R_y} = \frac{1}{\sqrt{3}R_w}(P^2 - P^3)$$
$$\mathbf{R_z} = \mathbf{R_x} \times \mathbf{R_y}.$$

As is the case with general parallel mechanisms, the forward kinematics solution is not unique. The initial guess is critical in the determination of the solution, particularly in the vicinity of singularities, where the algorithm may not always converge.

Algebraic Approach: In this section, we apply a method presented in [8] for solving the constraint equation (3) using an algebraic approach based on dialytic elimination.

Observe that (3) consists of three nonlinear equations in three unknowns. By applying the method developed in [8], we transform the constraint into polynomial form and eliminate unknowns in a clever way; this results in a 16th-order polynomial in one unknown whose solution can be completely characterized.

From the obtained values of the active and passive joints, the position and orientation of the tool frame can be found as in the numerical approach. One point of caution is that floating point overflow may occur in the computation due to the high order of the resultant.

Comparison: In general, the numerical approach has the advantage of simplicity and fast convergence for appropriate initial guesses, but has the disadvantages that only one root can be found, the algorithm may diverge near singularities, and is sensitive to choice of initial guess. The algebraic approach, on the other hand, has the advantage that all roots can be found, although the procedure for finding the analytic expression for the polynomial can be tedious. Finding all the roots of a polynomial can also be computationally expensive, and floating point overflow may occur due to the high order of the resultant (one means of alleviating this is to normalize the coefficients; in our case, the norm of the coefficient matrices in equations is normalized to be close to one). Also, picking out physically meaningful solutions from the roots of the polynomial depends on the particular application. Hence this procedure can be obscure and complicated in certain cases. In the case of the Eclipse, the physically correct solution is obtained by choosing the solution that is nearest to the current pose, since our primary interest is in solving the inverse kinematics along trajectories.

Table I shows the computational results of the two approaches, implemented in C++ on a 266-MHz Pentium PC. In order to obtain a meaningful comparison of the two methods, we measure the computation time for the values obtained from the inverse kinematic solution for end-effector postures uniformly distributed throughout the entire workspace (including orientation). 163 350 points in the workspace are taken for the numerical approach and 12 100 points for the algebraic approach. In the numerical approach, the initial guess was chosen as the solution perturbed by random functions whose ranges are $[-\pi, \pi]$ and $[-0.1\pi, 0.1\pi]$; we also set the maximum number of iterations to 50 and a convergence bound of 1E-9. In the algebraic approach, computation times for various parts of each procedure are shown in the table. We apply eigenvalue methods for the companion matrix constructed with the coefficients of the polynomial. The table reveals that the procedure for finding the roots of the polynomial consumes the most time; alternative algorithms should be able to improve overall performance significantly.

Our experience suggests that, in general, any choice between the two methods should be made based on the particular application. If all possible forward kinematic solutions are necessary, then it is worthwhile to invest the effort in obtaining the symbolic solution. If a solution needs to be obtained rapidly, then the numerical approach is to be preferred.

III. SINGULARITY ANALYSIS

Singularities are one of the most significant and critical problems in the design and control of parallel mechanisms. Unlike serial mechanisms, the consequences of venturing close to a singularity can be catastrophic for parallel mechanisms. Singularities for parallel mechanisms can be broadly classified into three

types (see [6]): 1) singularities of the joint configuration space (*configuration space singularity*); 2) configurations in which the mechanism loses one or more degrees of freedom as a result of the choice of actuated joints (*actuator singularity*); and 3) the mechanism's end-effector frame loses degrees of freedom of available motion (*end-effector singularity*). Actuator singularities can be further subclassified into *degenerate* and *nondegenerate* types: degenerate actuator singularities physically correspond to configurations in which some of the links can move even when the actuators are locked in place (i.e., self-motions of the mechanism), while nondegenerate singularities correspond to configurations in which certain actuator forces may cause internal forces in the mechanism.

For an m degree-of-freedom mechanism, its joint configuration space forms an m-dimensional surface in a higher-dimensional ambient space. The joint configuration space of the Eclipse is a six-dimensional surface (denoted $\mathcal{M}$) embedded in the ambient space $\mathcal{E} = \mathbb{R}^3 \times \mathbb{R}^3 \times T^3 \times SO(3)^3$; here $\mathbb{R}^3 \times \mathbb{R}^3 \times T^3$ denotes the joint space for the three circular prismatic joints, three linear prismatic joints, and three revolute joints, respectively, that are attached to each of the three serial structures. The configuration space for a ball-and-socket joint is taken to be $SO(3)$. Let $\mathcal{N}$ denote the n-dimensional manifold corresponding to the task space of the mechanism; for typical robotic applications $\mathcal{N}$ is taken to be the Special Euclidean group $SE(3)$, while for machining tasks, it is sufficient to take $\mathcal{N}$ as $\mathbb{R}^3 \times S^2$ since we are primarily interested in the direction of the spindle axis.

Let $\theta = (\theta_1, \ldots, \theta_k)$ and $u = (u_1, \ldots, u_m)$ denote local coordinates on $\mathcal{K}$ and $\mathcal{M}$, respectively. Since $\mathcal{M}$ is embedded in $\mathcal{K}$, θ can be written as a function of u, i.e., $\theta = \theta(u)$. Let $f = (f_1, \ldots, f_n)$ be local coordinates on $\mathcal{N}$, and also denote the forward kinematics f: $\mathcal{M} \rightarrow \mathcal{N}$ in local coordinates by $f(u)$. We use the notation $J = \nabla_u f$ to represent the derivative of f with respect to u. Now define a $k \times k$ diagonal matrix E such that it has 1s on the diagonal entries corresponding to the actuated joints, and all other entries 0. We also define the $m \times m$ matrix $G = (\nabla_u \theta)^T E (\nabla_u \theta)$.

Based on the above definitions, kinematic singularities can be classified into the following three types.

- **Configuration space singularities:** Configuration space singularities occur at boundaries of the configuration space manifold $\mathcal{M}$ and more generally at points of the configuration space manifold at which the tangent space is either ill-defined or no longer m-dimensional, e.g., self-intersections, or any ridges and folds on a surface. For example, if $\mathcal{M}$ is an m-dimensional surface embedded in $\mathcal{E} = \mathbb{R}^k$ and represented implicitly by the $k - m$ dimensional vector equation $\Phi(\theta) = 0$, then at a *regular point* $p \in \mathcal{M}$ [that is, a point at which the rank of $\nabla_\theta \Phi(p)$ is $k - m$] the rows of $\nabla_\theta \Phi(p)$ are vectors normal to the tangent space at p. However, at a singular point, its rank will be less than $k - m$, indicating a singular point of the manifold. In the case of the Eclipse, all of its configuration space singularities lie outside the workspace, and can be ignored.
- **Actuator singularities:** This case corresponds to the matrix G losing rank, i.e., rank $G < m$. Fig. 4 illustrates a nondegenerate actuator singularity for the Eclipse. In this configuration, the actuators are unable to resist certain applied generalized forces, or alternatively, internal forces can be generated. The particular actuator singularity occurs when the moving plate is at a tilting angle of approximately 30 degrees, such that one of the links lies in the same plane as the mobile plate and passes through the plate center.
- **End-effector singularities:** In this situation, the forward kinematics Jacobian loses rank: rank $J < n$. Physically this corresponds to the same notion of kinematic singularity for open chains, in which the end-effector loses one or more instantaneous degrees of freedom of motion. Fig. 5 shows an end-effector singularity for the Eclipse; here the moving platform is parallel to the fixed platform, and one of the spherical joints lies exactly above the center of the fixed platform. Physically, the end-effector singularity manifests itself by generating infinite velocities at a subset of the joints for certain infinitesimal motions of the end-effector frame (which in this case corresponds to the moving plate).

Fig. 4. A nondegenerate actuator singularity of the Eclipse.

Fig. 5. An end-effector singularity of the Eclipse.

Since for machining tasks one has a redundant degree of freedom afforded by rotation about the spindle axis, we can attempt to take advantage of this kinematic redundancy to avoid actuator singularities. Fig. 6 shows a plot of the condition number of G as a function of the tilting angle α and spindle axis rotation angle γ; here dark regions correspond to high values of the condition number, indicating an ill-conditioned G. As evident from the graph, the two actuator singularities at tilting angles of approximately 30 and 60 degrees are unavoidable—the two dark barriers corresponding to nondegenerate actuator singularities extend over the entire range of γ.

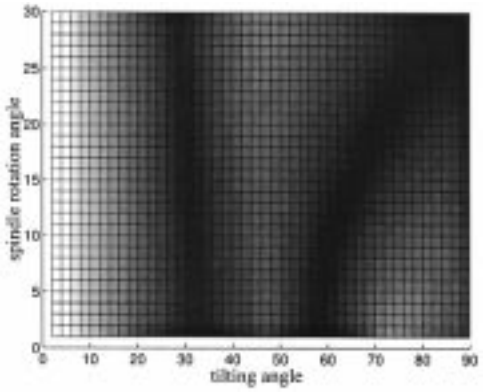

Fig. 6. Singularity barriers of the Eclipse.

Due to the presence of these unavoidable actuator singularities, the Eclipse is unable to tilt smoothly from 0 to 90 degrees; as the Eclipse passes instantaneously through such a singularity, there will be a noticeable jerk in the motion. A reasonable means of avoiding these singularities is to add extra actuators to the joints. To eliminate the two actuator singularity barriers, two additional actuators must be added [15]. We therefore add actuators to the revolute joint on the lower vertical column, and to the revolute joint on one of the upper vertical columns. The number of actuators (eight) now exceeds the kinematic mobility of the mechanism (six).

Obviously, the above actuation scheme without an appropriate control scheme can result in excessive internal forces. We adopt an independent joint control scheme; it has been shown in [14] that independent joint control tends to minimize internal forces generated by over-actuation. The practical consequences of adding redundant actuators to the mechanism are examined in more detail below.

IV. Workspace Analysis

The workspace of a mechanism refers to the set of all positions and orientations achievable by the end-effector frame. In the robotics literature, the workspace is often classified into two components, the *reachable* and *dexterous* workspace. The reachable workspace is defined to be the set of points in physical space that can be reached by the end-effector (or more precisely, the origin of the end-effector frame). The dexterous workspace, on the other hand, is the set of points that can be reached with any arbitrary orientation of the end-effector frame.

One disadvantage of this classification is that there is no means of smoothly trading off orientation freedom for position freedom. Differential geometric methods can overcome this disadvantage by introducing a natural volume form on the space of homogeneous transformations [13]. With this volume form, a geometric notion of workspace volume can be defined that has the advantage of being fixed and moving frame invariant, as well as being mathematically precise.

Parallel mechanisms that maximize this volume measure, however, are not necessarily well suited for machining applications. For example, in typical machining tasks, it is enough to require that the spindle be able to orient itself normally to the surface of the workpiece—it need not be able to assume general orientations at arbitrary points of the workspace. Also, the workpiece is usually placed at the center of the workspace, and spindle access to its bottom face is not necessary.

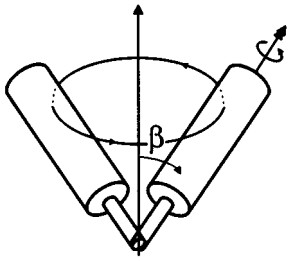

Fig. 7. Illustration of the concept of positioning workspace.

We now describe a notion of workspace that takes into account the special features of machining tasks. Suppose a reference frame is attached to the spindle in such a fashion that the z axis is directed along the spindle axis. Define the rotation angles about the x, y, and z axes by α, β, and γ. Borrowing machine tool terminology, we shall also refer to α, β, and γ as the spindle *turning, tilting,* and *rotation* angles, respectively. Note that the rotation angle γ is irrelevant for machining purposes and can be regarded as a redundant degree of freedom. The z axis of the fixed frame is assumed to be directed vertically upward.

Given a mechanism, the *positioning workspace for spindle tilting angle* β is now defined to be the set of all points in Cartesian space with respect to which the spindle can rotate 360° about the fixed frame z axis (with the spindle tip maintaining contact with the point in question), while the spindle is tilted at an angle of β with respect to the vertical ($\beta = 0°$ indicates a vertical spindle, suitable for machining the top surface of the cube, while β should be set to 90° in order to machine the side faces). Fig. 7 graphically illustrates this concept of positioning workspace. Because of mechanical constraints most existing parallel mechanism designs have a limited spindle tilting angle, typically a maximum β of approximately 40°.

To calculate the machine tool workspace as described above for actual mechanisms, it is extremely important (especially for parallel mechanisms) to keep in mind the physical constraints at work: joint limits for prismatic, revolute, and spherical joints, as well as interference between the links. Of the three types of joints considered, our experience suggests that in general spherical joint limits tend to be the most dominant in determining a mechanism's workspace. Figs. 8 and 9 illustrate the positioning workspace of the Eclipse for tilting angles of 0 and 90 degrees, respectively, where the spherical joints are assumed to have a joint range of $\pm 55°$.

Another important consideration in assessing a mechanism's workspace capabilities is its topological properties, particularly its connectedness. For example, although a mechanism may be able to access all five faces of a cube, it may not be possible to track a closed path that traverses all five faces without breaking contact. A useful human analogy is to trace a vertical path down one's back with one hand; for the upper portion of the path one would reach over the shoulder with the arm, while for the lower portion one would wrap the arm around the waist and reach up. For the Eclipse, it can be experimentally verified that the workspace is topologically simply connected and that all

Fig. 8. Positioning workspace for tilting angle of 0 degrees.

Fig. 9. Positioning workspace for tilting angle of 90 degrees.

closed paths in its workspace can be traced without breaking contact.

V. Stiffness Analysis

The overall stiffness of a mechanism is determined both by joint and link deflections. Depending on the mechanism, the relative contributions of these deflections may vary considerably. Assuming linear models of joint deflection, joint stiffness can be modeled quite easily within the framework of *manipulability* [10], [11]. The qualitative idea behind the concept of manipulability is the ability of a mechanism to move and apply forces in arbitrary directions as easily as possible. The major axis of the manipulability ellipsoid indicates the direction along which the mechanism can move with the least effort, while the minor axis indicates the direction along which the mechanism is stiffest, i.e., the mechanism's actuators can resist forces with minimum effort along these directions. Link structural stiffness analysis on the other hand, which is more difficult to model and has received only limited attention in the literature, is essential to determining various design parameters like a link's length, inertia, and cross-sectional area. For accurate stiffness analysis of parallel mechanisms, it is necessary to consider both types of deflections.

In previous research on the structural stiffness of Stewart platforms [18], the platform's structural stiffness is usually only affected by axial forces along the legs, since one of the joints connecting each link to the two platforms is a spherical joint—link structural stiffness in this situation essentially corresponds to joint stiffness. For more general parallel mechanisms like the Eclipse, one must also consider bending and torsional moments. While in principle an FEM analysis will reveal complete information on a machine's structural stiffness, such a procedure is time-consuming and expensive. At the design stage, it would be more desirable to have an efficient first-order method of stiffness analysis that places both kinematic and elastic effects on an even footing.

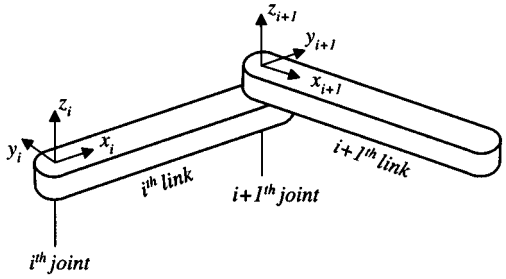

Fig. 10. Serial chain compliance: definition of link frames.

With these goals in mind, we focus here on the structural *compliance* of a parallel mechanism. For the case in which the number of actuators equals the kinematic mobility of the mechanism, the mechanism's structural compliance can be defined in terms of the structural compliance of the individual serial chains that compose the mechanism. Toward this end, we begin with an elasto-kinematic analysis of an n-link serial chain. Suppose that reference frames are attached to each link as shown in Fig. 10. We assume that each link can be modeled as a slender rod; hence, when an external force is applied to the link, one need only consider bending and torsional moments together with the axial force. Observe that the link frames are attached such that moments about the x axis act as a torsional moment, and moments about axes lying in the y–z plane act as a bending moment. By choosing the x axis to lie along the length of the link, we can decouple the elastic behaviors due to torsion and bending moments.

Suppose an external force f and external moment m are applied to the tool tip; here both vectors are expressed in tool frame coordinates. In what follows, we combine moments and forces and express them as a single generalized force, i.e., $\mathcal{F} = (m,\ f)$. The moment and force experienced at the ith link frame, $(m_i,\ f_i) = \mathcal{F}_i$, is then given by

$$\mathcal{F}_i = Ad^*_{T_i} \begin{bmatrix} m \\ f \end{bmatrix}$$

where

$$T_i = \begin{bmatrix} R_i & p_i \\ 0 & 1 \end{bmatrix}$$

is the homogeneous transform representing the ith link frame relative to the tool frame, and

$$Ad^*_{T_i} = \begin{bmatrix} R_i & 0 \\ [p_i]R_i & R_i \end{bmatrix}^T$$

$$[p_i] = \begin{bmatrix} 0 & -p_{i,z} & p_{i,y} \\ p_{i,z} & 0 & -p_{i,x} \\ -p_{i,y} & p_{i,x} & 0 \end{bmatrix}.$$

The strain energy of the ith link due to the generalized external force $\mathcal{F}$ can then be expressed as follows:

$$U_{i,b} = \tfrac{1}{2}\int_0^1 m_{i,b}(s)^T W_i^{-1} m_{i,b}(s)\, ds$$
$$m_{i,b}(s) = [\,-Id \quad [p_{i,i+1}]s\,]\, Ad^*_{T_i}\mathcal{F}$$
$$W_i = \begin{bmatrix} G_iJ_i & 0 & 0 \\ 0 & E_iI_{i,yy} & E_iI_{i,yz} \\ 0 & E_iI_{i,zy} & E_iI_{i,zz} \end{bmatrix}$$

where Id denotes the 3×3 identity matrix, and for each link i, G_i is the shear modulus, J_i is the polar moment of area, E_i is the Young's modulus of the link material, and I_i is the second moment of area. $p_{i,i+1}$ is the vector from the ith frame origin to the $(i+1)$ frame origin. From the link frame assignment convention as shown in Fig. 10, $p_{i,i+1}$ can be expressed simply as $[L_i\ 0\ 0]^T$, where L_i denotes the length of link i.

After some calculation, the energy can be expressed as

$$U_{i,b} = \frac{1}{2}\mathcal{F}^T C_{i,b}\mathcal{F}$$
$$C_{i,b} = {Ad^*_{T_i}}^T \cdot \begin{bmatrix} W_i^{-1} & -\frac{1}{2}W_i^{-1}[p_{i,i+1}] \\ -\frac{1}{2}[p_{i,i+1}]^T W_i^{-1} & \frac{1}{3}[p_{i,i+1}]^T W_i^{-1}[p_{i,i+1}] \end{bmatrix} Ad^*_{T_i}.$$

From Castigliano's Theorem, the total deflection due to bending is given by

$$\begin{bmatrix} \delta\Omega_b \\ \delta x_b \end{bmatrix} = \frac{\partial U_b}{\partial \mathcal{F}} = C_b\mathcal{F}$$

where $C_b = \sum_{i=1}^N C_{i,b}$. Note that $\delta\Omega$ above is a vector representation of the 3×3 skew-symmetric matrix $R^T\delta R$ that corresponds to the infinitesimal angular displacement of the tool frame expressed in tool frame coordinates. δx is the Cartesian displacement, also expressed in tool frame coordinates.

In a similar fashion, the deflection due to axial forces can be written as

$$\begin{bmatrix} \delta\Omega_a \\ \delta x_a \end{bmatrix} = C_t\mathcal{F}$$

where

$$C_t = \sum_{i=1}^N C_{i,t}$$
$$C_{i,t} = \frac{1}{E_iA_iL_i}\, {Ad^*_{T_i}}^T \begin{bmatrix} 0 & 0 \\ 0 & p_{i,i+1}p_{i,i+1}^T \end{bmatrix} Ad^*_{T_i}$$

where A_i and L_i are, respectively, the cross-sectional area and link length of link i, and 0 is the 3×3 zero matrix. The structural stiffness matrix of the open chain can now be obtained as the inverse of its structural compliance matrix, i.e., $K = (C_b + C_t)^{-1}$; the relation between the tip displacement $(\delta\Omega,\ \delta x)$ and the external generalized force $\mathcal{F}$ is given by

$$\mathcal{F} = K\begin{bmatrix} \delta\Omega \\ \delta x \end{bmatrix}.$$

We now consider closed chains, whose analysis is is complicated by the fact that, unlike open chains, they typically possess passive joints that are not actuated. However, a large class of closed chain systems including the Eclipse have the common feature of one moving plate supported by several serial sublinkages. Typically spherical joints are used to connect the moving plate with each of the sublinkages. For our analysis we will address closed chains having such a parallel structure. The key idea then is to decompose the original system into a set of multiple open chains whose motions are restricted by a kinematic constraint. We assume that the moving plate and the base circular guide are completely rigid. In practice, it is expected that the elastic behaviors of the base ring gear and ball screw sliding guide will have some effect on the overall machine stiffness. Our informal experience indicates, however, that for our design purposes these effects can be neglected in comparison with the flexibility of the vertical columns and fixed links. Under static equilibrium, given a generalized force acting on the tool tip it is possible to calculate the reactive forces at the spherical joints. These forces are in turn generated by reactive forces along the link axial direction, as well as the direction of the revolute joint axis to which one end of the link is attached.

For link i, let d_i and b_i denote unit vectors along the link axial direction and the rotational joint axis, respectively, and let p_i, q_i denote their respective force magnitudes. Then the resultant force generated at the ith spherical joint by these forces is $p_id_i + q_ib_i$. Under static equilibrium, we have

$$\mathcal{F} = D[\,p_1 \quad q_1 \quad p_2 \quad q_2 \quad p_3 \quad q_3\,]^T$$

where

$$D = \begin{bmatrix} r_1\times d_1 & r_1\times b_1 & r_2\times d_2 & r_2\times b_2 & r_3\times d_3 & r_3\times b_3 \\ d_1 & b_1 & d_2 & b_2 & d_2 & b_2 \end{bmatrix}.$$

Assuming the mechanism is not at an actuator singularity, D will be nonsingular. The resultant force at the ith spherical joint will then be

$$\mathcal{F}_i = \begin{bmatrix} 0 \\ p_id_i + q_ib_i \end{bmatrix} = \begin{bmatrix} 0 \\ D_iS_iD^{-1} \end{bmatrix}\mathcal{F}$$

where $D_i = [\,d_i \quad b_i\,]$, and S_i is a selection matrix composed of 1s and 0s; for example,

$$S_1 = \begin{bmatrix} 1 & 0 & 0 & 0 & 0 & 0 \\ 0 & 1 & 0 & 0 & 0 & 0 \end{bmatrix}$$

selects the magnitudes p_1, q_1 corresponding to the reactive forces at the first spherical joint.

Given an external generalized force $\mathcal{F}$ applied to the tool tip, the reactive generalized forces $\mathcal{F}_i$ at the three spherical joints can now be computed as above. The total strain energy due to the external generalized force can be expressed as

$$U = \sum_{i=1}^3 \frac{1}{2}\mathcal{F}_i^T C_i\mathcal{F}_i$$

(a) (b)

Fig. 11. Compliance ellipsoids for tilting angle 0°. (a) Structural compliance ellipsoid. (b) Joint compliance ellipsoid.

(a) (b)

Fig. 12. Compliance ellipsoids for tilting angle 90°. (a) Structural compliance ellipsoid. (b) Joint compliance ellipsoid.

where C_i is the structural compliance matrix for the ith subchain. Then the total structural compliance matrix of the mechanism can be defined as

$$\begin{bmatrix} \delta\Omega \\ \delta x \end{bmatrix} = \mathcal{C}\mathcal{F}$$

where

$$\mathcal{C} = \sum_{i=1}^{3} \mathcal{D}_i^T C_i \mathcal{D}_i$$

$$\mathcal{D}_i = \begin{bmatrix} 0 \\ D_i S_i D^{-1} \end{bmatrix}.$$

The above formulation will hold for determinate systems, i.e., systems in which the relation between the generalized external force and the generalized reactant forces can be solved under static equilibrium conditions. Although the Eclipse is indeterminate due to its redundant actuators, for structural reasons one employs a control strategy that attempts to generate as little internal forces as possible. Therefore, the above formulation provides a reasonable analysis of the structural stiffness behavior of the Eclipse.

Figs. 11 and 12 illustrate the joint and structural compliance ellipsoids at the two extreme configurations for the Eclipse. Although compliance and stiffness matrices are by definition six-by-six, in many cases it is quite sufficient to consider only the position-force relationship (particularly for machining applications, where the spindle tip's contact with the workpiece is often modeled as a frictionless point contact.

For our analysis, we focus on the right-lower 3×3 submatrix of the compliance matrix, which corresponds to the Cartesian position-force stiffness. The principal axes of the ellipsoids indicate the direction and magnitude of the deflections of the end-effector for a unit external force, with the magnitudes and associated force directions as given in Table II. The magnitudes of the elements in the joint compliance matrices should be interpreted as relative values, whereas those of the structural compliance matrices are absolute values. Fig. 13 depicts the Frobenius norm of the 3×3 joint and structural compliance submatrices (corresponding to Cartesian position-force stiffness) for different locations of the tool tip in the x–y plane.

An analysis of the above type is clearly useful, even essential, in determining the radius of the links—stiffness analysis does not provide useful information in this regard.

Fig. 14 shows the compliance measure as a function of the link radius. In the graphs, the x, y, and z axes correspond to variations in the radii of the first, second, and third links, respectively. Our analysis results suggest that at tilting angle 0 °,

TABLE II
MAGNITUDES OF ELLIPSOIDS AND ASSOCIATED FORCE DIRECTIONS

structural compliance ellipsoid at tilting angle 0°	
F_{max}	[0.8688 , 0 , 0.4962]
F_{min}	[0.4952 , 0 , 0.8688]
magnitudes	1E-5×[0.1545 , 0.1198 , 0.013]
joint compliance ellipsoid at tilting angle 0°	
F_{max}	[0.6338 , 0.538 , 0.5557]
F_{min}	[-0.7734 , 0.4333 , 0.4627]
magnitudes	[3.7185 , 0.8833 , 0.0906]
structural compliance ellipsoid at tilting angle 90°	
F_{max}	[0 , 1 , 0]
F_{min}	[-0.1739 , 0 , 0.9848]
magnitudes	1E-5×[0.3489 , 0.0490 , 0.0244]
joint compliance ellipsoid at tilting angle 90°	
F_{max}	[0.9409 , -0.0454 , 0.3357]
F_{min}	[-0.3241 , -0.4088 , 0.8531]
magnitudes	[8.4256 , 1.8359 , 0.7431]

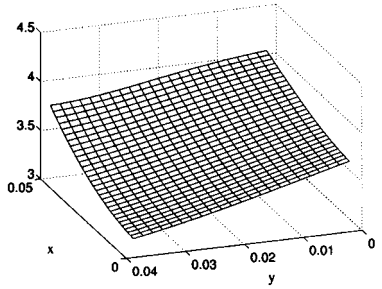

Fig. 13. Frobenius norm of the joint and structural compliance submatrices corresponding to Cartesian position-force stiffness.

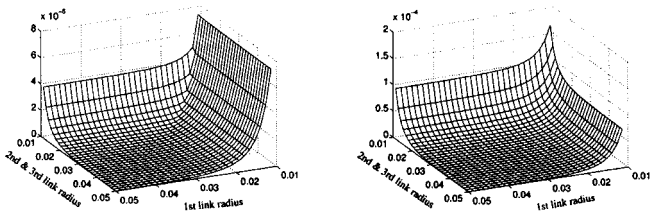

(a) (b)

Fig. 14. The compliance measure as a function of the link radius. (a) At tilting angle 0 °. (b) At tilting angle 90 °.

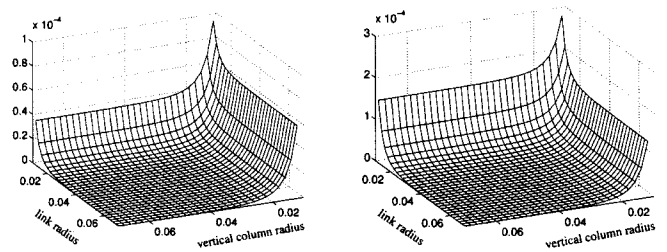

(a) (b)

Fig. 15. The compliance measure as a function of the link radius and the vertical column radius. (a) At tilting angle 0 °. (b) At tilting angle 90 °.

Fig. 16. The Eclipse prototype.

the machine's stiffness is most sensitive to variations in the first link radius, while for a tilting angle of 90°, the machine's stiffness is more sensitive to the radii of the remaining two links. The stiffness sensitivity becomes sufficiently small when the radius of each link exceeds 35 mm; for the prototype, the link radius is chosen to be 33 mm.

Fig. 15 shows the compliance measure as a function of the link radius and the vertical column radius. Although the vertical column of the actual Eclipse prototype has a rectangular cross section, for our present purposes we assume a circular cross section. The x axis corresponds to the link radius, while the y axis corresponds to the vertical column radius.

VI. Development of the Prototype Eclipse

An experimental prototype, shown in Fig. 16, has been constructed to verify the viability of the Eclipse architecture as a five-face machining center. It consists of three vertical columns, each of which slides independently on a pair of circular guide bearings of diameter of 500 and 600 mm, respectively. The shape of the workspace is a cylinder, the diameter and height of which are 100 mm. The maximum feedrate of the tool tip is 1.5 m/min. The movement of each column along the circular bed

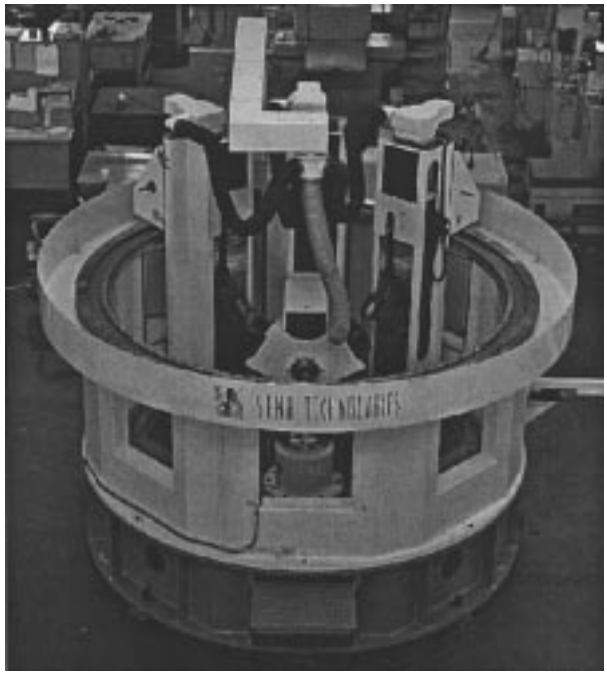

Fig. 17. The Eclipse machine.

is achieved by a servomotor and a pinion and ring gear transmission. Each column has a carriage, which moves vertically along the linear slideway of the column. The carriage movement is achieved by the servomotor and a ball screw transmission. A fixed link is attached to each of the carriages through a pin joint. The other end of the fixed link is attached to the tool spindle plate via a ball-socket joint. Also, the R joint on the lower vertical column is also actuated by a harmonic drive.

The prototype also has a vertical workpiece spindle unit in the middle span of the machine, where the workpiece is fixed. For turning and grinding processes, the vertical workpiece spindle can be rotated to achieve spinning of the workpiece. In this case the tool spindle can be fixed to maintain a horizontal posture for turning processes; this is equivalent to a vertical turning process. For grinding processes, the tool spindle is also rotated. For the cases of general milling, drilling, boring and tapping processes, the vertical workpiece spindle unit is fixed, and only the tool spindle is rotated. In this way the prototype machine can accommodate turning, milling, and grinding processes all within the same platform.

It is to be noted that the tip of the tool spindle can move freely from the vertical posture to the horizontal posture and vice versa. Hence, it can realize five-face milling processes within a single setup. To cut the upper surface of the workpiece, the tool spindle moves to the vertical posture and to the horizontal posture for cutting side surfaces. All four side surfaces can be cut without any indexing mechanism along the B axis, since the tool spindle itself is able to move around the workpiece. It should also be noted that actually the prototype machine can execute simultaneous five-axis machining at any tool posture ranges from vertical to horizontal. This advantage can extend the machining ability of the free surface to a wider workspace.

Since the design objective of the redundantly actuated Eclipse prototype was to verify the performance of the newly created parallel mechanism, the stiffness was not a main issue at this

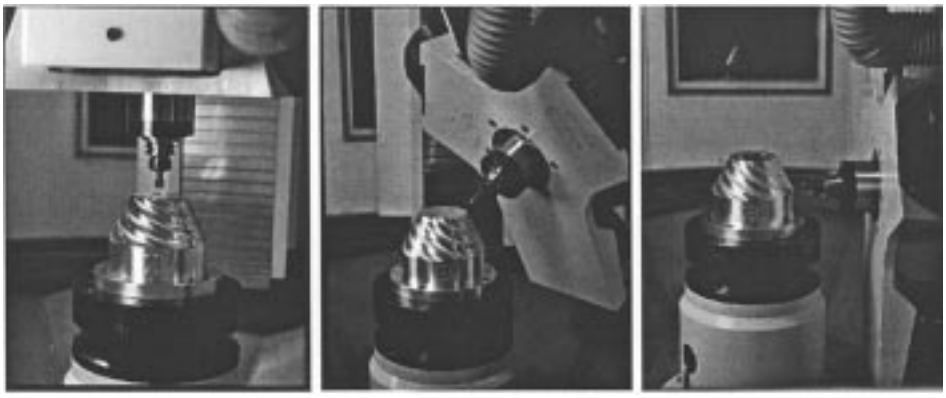

Fig. 18. The Eclipse machine shown machining aluminum stock.

stage. At the vertical posture, stiffness is 1.2 and 0.6 N/μm along the spindle axis and radial direction, respectively. At the horizontal posture, stiffness is 1.5 and 3.0 N/μm along the spindle axis and radial direction, respectively. With this stiffness, we could only machine plastic samples.

VII. Development of the Eclipse Machine

Once the performance of the Eclipse mechanism was verified, a real machine was designed and constructed. Fig. 17 shows the photography of the Eclipse machine. Diameters of a pair of circular guide bearings are 2400 mm and 2600 mm, respectively. The workspace is $\phi 300 \times 200$. The maximum feedrate of the tool tip is 3.3 m/min and the maximum acceleration of the tool tip is 0.1 G. The rated power and maximum speed of the tool spindle is 2.2 kW and 4000 rpm. And the rated power and maximum speed of the workpiece spindle is 15 kW and 3000 rpm.

It has three special features when compared to the Eclipse prototype.

1) All three vertical columns are directed upward from the base ring and with each other. In contrast, the Eclipse prototype has one vertical column downward from the base ring to avoid the interference between the fixed link and the workpiece at the horizontal posture. At the initial design stage of the Eclipse machine, we optimized the mechanism's kinematic parameters and were able to eliminate the interference problem.
2) Universal joints are substituted for the ball-socket joints in the Eclipse prototype, to improve stiffness.
3) The machine controller, an open architecture PC-based CNC, is specially developed for the Eclipse machine.

The Eclipse machine was designed for the metal cutting process and the stiffness of the machine is an important issue. At the vertical posture, stiffness is 18.2 N/μm and 13.8 N/μm along the spindle axis and radial direction, respectively. At the horizontal posture, stiffness is 1.1 N/μm and 5.8 N/μm along the spindle axis and radial direction, respectively. At the vertical posture, the Eclipse machine is much stiffer than the Eclipse prototype. However, at the horizontal posture, the stiffness of the Eclipse machine is of the same order with the Eclipse prototype. This is because one downward vertical column structure of the Eclipse prototype is superior to three upward vertical column structure of the Eclipse machine at the horizontal posture. With this stiffness, we could successfully machine aluminum stock. Fig. 18 shows the Eclipse machine that is machining the aluminum stock at the vertical posture, tilted posture and horizontal posture in turn.

VIII. Conclusion

When the actuator on the R joint of the lower vertical column is removed, there exists an unavoidable actuator singularity at tilting angles of approximately 30 and 60 degrees. While the singularities indicated earlier can be avoided by a judicious choice of the spindle angle γ, these two singularities unfortunately cannot be avoided with the extra redundancy. It is precisely to overcome this singularity problem that we have added an actuator to the R joint of the lower vertical column. It seems that redundantly actuated structures are the only viable means of achieving our machining goals while avoiding kinematic singularities. Preliminary analysis results indicate that the presence of redundant actuation in fact may even improve the overall stiffness of the mechanism.

The Eclipse mechanism fulfills all the multi-process machine requirements set forth earlier, namely, five-face machining and simultaneous five-axis machining. The singularity problem can be remedied by simply adding an actuator to the lower column unit. The Eclipse realizes these capabilities within a single machine tool and can serve as a platform for a rapid machining system that can significantly reduce machining lead time by eliminating unnecessary workpiece setup times. Although singularities can be avoided by redundant actuation, one must now be careful in controlling the mechanism. Our present research efforts are directed at designing control algorithms for redundantly actuated systems like the Eclipse, as well as methods for kinematic calibration and dynamic modeling.

Future research on motion planning for redundantly actuated systems with kinematic redundancy: maximizing stiffness as a means of kinematic redundancy resolution, and of torque distribution. e.g., motion planning and control for maximizing stiffness, dynamics of redundantly actuated closed chains containing both active and passive joints, methods for optimal torque distribution, etc. Our experience strengthens our belief that parallel mechanisms are most useful when designed with a specific task in mind, and not as a universal mechanical platform.

References

[1] J. P. Merlet, "Parallel manipulators: State of the art and perspectives," *Adv. Robot.*, vol. 8, no. 6, pp. 589–598, 1994.

[2] F. Pierrot, P. Dauchez, and A. Fournier, "Fast parallel robots," *J. Robot. Syst.*, vol. 8, no. 6, pp. 829–840, 1991.
[3] C. Ferraresi *et al.*, "Static and dynamic behavoir of a high stiffness Stewart platform-based force/torque sensor," *J. Robot. Syst.*, vol. 12, no. 12, pp. 883–893.
[4] M. Valenti, "Machine tools get smarter," *ASME Mech. Eng.*, vol. 117, no. 11, pp. 70–75, Nov. 1995.
[5] J. W. Kim *et al.*, "Performance analysis of parallel manipulator architectures for CNC machining," in *Proc. 1997 ASME IMECE Symp. on Machine Tools*, Dallas, TX, 1997.
[6] F. C. Park and J. W. Kim, "Singularity analysis of closed kinematic chains," *ASME J. Mechanical Design*, vol. 121, no. 1, pp. 32–38, 1999.
[7] R. Matone and B. Roth, "A framework on how to model actuation schemes and a study of their effects on singular postures," *ASME J. Mech. Design*, vol. 121, no. 1, pp. 2–8, 1999.
[8] J. Kim and F. C. Park, "Direct kinematic analysis of 3-RS parallel mechanisms," Mechanism and Machine Theory, 2001, to be published.
[9] G. R. Dunlop and T. P. Jones, "Position analysis of a 3-DOF parallel manipulator," *Mechanism Mach. Theory*, vol. 32, no. 8, pp. 903–920, 1997.
[10] F. C. Park and J. W. Kim, "Manipulability of closed kinematic chains," *ASME J. Mech. Design*, vol. 120, no. 4, pp. 542–548, 1998.
[11] T. Yoshikawa, "Manipulability of robotic mechanisms," *Int. J. Robot. Res.*, vol. 4, no. 2, pp. 3–9, 1985.
[12] C. Gosselin, "Determination of the workspace of 6-dof parallel manipulators," *ASME J. Mech. Design*, vol. 112, no. 3, pp. 331–336, 1990.
[13] J. Loncaric, "Normal forms of stiffness and compliance matrices," *IEEE J. Robot. Automat.*, vol. RA-3, pp. 567–572, Dec. 1987.
[14] G. R. Luecke and J. F. Gardner, "Experimental results for force distribution in cooperating manipulator systems using local joint control," *Int. J. Robot. Res.*, vol. 13, no. 6, pp. 471–480, 1994.
[15] B. Dasgupta and T. S. Mruthyunjaya, "Force redundancy in parallel manipulators: theoretical and practical issues," *Mechanism Mach. Theory*, vol. 33, pp. 727–742, 1998.
[16] J. P. Merlet, "Determination of 6D workspaces of Gough-type parallel manipulator and comparison between different geometries," *Int. J. Robot. Res.*, vol. 18, no. 9, pp. 902–916, 1999.
[17] D. Stewart, "A platform with six degrees of freedom," *Proc. Inst. Mech. Eng.*, pt. I, vol. 180, no. 15, pp. 371–386, 1966.
[18] S. Bhattarchaya, H. Hatwal, and A. Ghosh, "On the optimum design of Stewart platform type parallel manipulators," *Robotica*, vol. 13, pp. 133–140, 1995.

Jongwon Kim received the B.S. degree in mechanical engineering from Seoul National University, Seoul, Korea, in 1978, the M.S. degree from KAIST, Korea, in 1980, and the Ph.D. degree from the University of Wisconsin—Madison in 1987.

He is currently an Associate Professor in the School of Mechanical and Aerospace Engineering at Seoul National University in Korea. He worked as a Senior Manager at Daewoo Heavy Industries, Ltd. His research interests are in intelligent manufacturing systems and parallel kinematic machines.

Dr. Kim received the Best Paper Award from ASME Manufacturing Engineering Division in 1997 and SME University LEAD Award in 1996.

Frank Chongwoo Park received the B.S. degree in electrical engineering and computer science from the Massachusetts Institute of Technology, Cambridge, in 1985 and the S.M. and Ph.D. degrees in applied mathematics from Harvard University, Cambridge, MA, in 1988 and 1991, respectively.

In 1988, he was a Researcher in the Manufacturing Research Group of the IBM T.J. Watson Research Center. From 1991 to 1995, he was an Assistant Professor of Mechanical and Aerospace Engineering at the University of California, Irvine. Since 1995, he has been at the School of Mechanical and Aerospace Engineering at Seoul National University, where he is currently an Associate Professor. His research interests are in the broad areas of robotics, mathematical systems theory, and related areas of applied mathematics.

Dr. Park currently serves as an Associate Editor of the IEEE TRANSACTIONS ON ROBOTICS AND AUTOMATION.

Sun Joong Ryu received the B.S., M.S., and Ph.D. degrees in mechanical engineering from Seoul National University, Korea, in 1994, 1996, and 2001, respectively.

His research interests include design, kinematics, dynamics, and control of parallel mechanisms. He has participated in the development of redundantly actuated six-degrees-of-freedom parallel mechanism—the Eclipse—since 1997 at the Seoul National University, Korea.

Jinwook Kim received the B.S. and M.S. degrees in mechanical engineering from Seoul National University, Seoul, Korea, in 1995 and 1997, respectively. He is currently working toward the Ph.D. degree at the same university.

His research interests include parallel mechanism kinematics, multibody system dynamics, and development of general robot simulation software.

Jae Chul Hwang received the B.S. and M.S. degrees in mechanical engineering from Seoul National University, Seoul, Korea, in 1996 and 1998, respectively. He is currently working toward the Ph.D. degree at the same university.

From 1998 to 2000, he worked as a Researcher at the Engineering Research Center for Advanced Control and Instrumentation. His research interests include kinematics, dynamics, and control of parallel kinematic machines.

Changbeom Park received the B.S. and M.S. degrees in mechanical engineering from Seoul National University, Seoul, Korea, in 1996 and 1998, respectively.

He is currently with the Intelligent Mechanical System Research Department of Hyundai Heavy Industries. His research interests are development of industrial robot system and off line programming system for robots.

Cornel C. Iurascu received the M.S. degree in mechanical engineering from the University "Politehnica" Bucharest, Romania, and the Ph.D. degree from Seoul National University, Seoul, Korea, with a research specialization in the area of robotics and manufacturing.

From 1991 to 1995, he was a Lecturer with the University "Politehnica" Bucharest. He is presently a Post-Doctoral Fellow in the School of Mechanical and Aerospace Engineering at Seoul National. His current research and teaching interests include kinematics and dynamics of serial and parallel mechanisms, kinematic and dynamic calibration, design optimization, geometric algorithms, CAD, control systems for automated machines, and mechatronics.